Analysis of Flow Pattern Transition from Segregated to Slug flow in Upward Inclined Pipes

Fan, Y.; Pereyra, E.; Sarica, C.; Schleicher, E.; Hampel, U.;

Originally published:

June 2019

International Journal of Multiphase Flow 115(2019), 19-39

DOI: https://doi.org/10.1016/j.ijmultiphaseflow.2019.03.021

Perma-Link to Publication Repository of HZDR:

https://www.hzdr.de/publications/Publ-27867

Detailed Analysis of Flow Pattern Transition from Segregated to Slug flow in Upward Inclined Pipes

Yilin Fan[1], Eduardo Pereyra[2], Cem Sarica[2], Eckhard Schleicher[3] and Uwe Hampel[3]
[1]*Petroleum Engineering Department, Colorado School of Mines, CO 80401, USA*
[2]*McDougall School of Petroleum Engineering, The University of Tulsa, Tulsa, OK 74104, USA*
[3]*Institute of Fluid Dynamics, Helmholtz-Zentrum Dresden-Rossendorf (HZDR), Germany*

Abstract

Segregated and slug flows are two of the most common flow patterns encountered in two-phase upward inclined pipe flow. However, the transition between them is ambiguous. Coherent and distinctive structures have been observed within the transition. These structures have been classified as pseudo-slug flow. The nature of pseudo-slug flow is not well understood due to the complexity of the structure. At low liquid loading conditions, this flow pattern can occupy a large operating region and cannot be neglected. This paper presents a detailed experimental work conducted in a facility with a valley configuration, focusing on the transition region between segregated and slug flows. Wire-mesh sensors were employed to investigate the liquid phase distribution within the flow structure.

The current paper investigates the flow patterns and their transition in upward inclined pipe from different perspectives. The investigation includes analysis of images from high-speed videos, evaluation of 2-D liquid holdup axial evolution, 2-D liquid holdup distribution at pipe cross-section, 3-D interfacial structure evolution, and analysis of pressure gradient and liquid holdup measurement, flow characteristics, etc. Differences between slug and pseudo-slug flows are also presented.

Three superficial liquid velocities (0.001, 0.005 and 0.01 m/s) and five inclination angles (2°, 5°, 10°, 15°, and 20°) are studied. Simplified correlations are proposed for pseudo-slug structural velocity, showing fair agreement.

Keywords: Pseudo-slug Flow, Flow Pattern Transition, Two-phase Flow in Inclined Pipe, Wire-mesh Sensor, Low Liquid Loading

1. Introduction

Segregate (SEG) and slug (SL) flow are the two most common flow patterns encountered in the oil and gas industry. They neighbor each other in commonly known flow pattern maps for two-phase upward inclined pipe flow (Barnea 1987; Zhang *et al*., 2003). However, the transition from segregated flow to slug flow does not occur abruptly. There is a transition region between them, which has been named differently amongst the researchers.

The transition was recognized by Nicholson *et al*. (1977) and it was named as "proto-slug". Barnea *et al*. (1980) defined it as "wavy-annular" flow. Lin and Hanratty (1987b) later provided a detailed description of this flow pattern, and named it as "pseudo-slug" flow, which is the term adopted in the current study. They also stated that the pseudo-slugs observed in the 2.54 cm pipe resemble the "disturbance wave" described by Butterworth and Pulling (1972) and the picture of a "slug" presented in the paper by Alves (1954). The pseudo-slug flow was classified into "intermittent flow" together with slug and plug flows in Taitel and Dukler (1976) flow pattern transition model.

Lin and Hanratty (1987b) conducted an experimental study of air-water flow in horizontal pipes with two different diameters. They defined the pseudo-slugs as: "The disturbances, which have the appearance of slugs, but which do not give the identifying pressure pattern and do not travel at the gas velocity. The pseudo-slug flow pattern resembles; annular flow in that a continuous liquid film is formed on the pipe circumference; wavy-stratified flow in that a thick layer of liquid is present at the bottom of the pipe; and slug flow in that large slug-like structures capable of reaching the top of the pipe are present." In their experiment, they observed large, ill-defined waves in the pseudo-slug body, which could touch the top wall shortly, but did not block the entire cross-sectional area of the pipe as slugs did. A large void was observed in the upper portion of the pseudo-slugs.

There were many other studies reported the observation of pseudo-slug flow in horizontal pipes under high liquid flow rate conditions such as Lee (1993), Soleimani and Hanratty (2003) and Loh *et al*. (2016). Pseudo-slug flow was also reported near the transition from segregated to slug flows in upward inclined pipes with $\theta < 30°$ (Wilkens, 1997; Maley, 1997; Alsaadi, 2013, 2015; Ekinci, 2015 and Brito, 2015, 2016). Similar with the observations of Lin and Hanratty (1987a, b), the translational velocity of pseudo-slugs was smaller than that expected for slugs in all of these studies. Wilkens (1997) and Maley (1997) also showed that the slug flow pattern became dominated by pseudo-slug flow as the pressure was increased. Alsaadi (2013, 2015) conducted an experimental study in 3-in low pressure upward inclined pipes (2° ~ 30°) using air and tap water. He observed a significant occurrence of pseudo-slug flow in his experiments. Moreover, Ekinci (2015) conducted experiments on slug flow characterization for high-viscosity oil and gas flow in ±2° inclined pipe, and reported pseudo-slug flow at high gas flow rates.

It can be concluded from the previous studies that pseudo-slug flow pattern exists near the transition from segregated flow to slug flow for horizontal and upward inclined pipe, and its topological structure is quite different from that of slug flow. This flow pattern can occupy a large region on a flow pattern map at low liquid flow conditions or high-viscosity oil and air flow in an upward inclined pipe. However, none of the previous studies provided a detailed study on pseudo-slug flow. To better understand this flow pattern, wire-mesh sensors were employed in the current study to investigate the liquid phase distribution within the flow structure. This paper provides a detailed analysis of images from high-speed videos, evaluation of 2-D liquid holdup axial evolution, 2-D liquid holdup distribution at pipe cross-section and 3-D interfacial structure evolution, and analysis of pressure gradient and liquid holdup measurement, and structure velocities.

Three superficial liquid velocities (0.001, 0.005 and 0.01 m/s) and five inclination angles (2°, 5°, 10°, 15°, and 20°) are studied. Simplified correlations are proposed for pseudo-slug structural velocity, which can be easily applied in pseudo-slug mechanics model.

2. Experimental Facility

The Tulsa University Fluid Flow Projects (TUFFP) low-pressure air/water 0.0762 m ID facility was used in this experimental study. The schematic of the facility is shown in Fig. 1. Tulsa city municipal water and compressed air were used as the test fluids. The air was compressed by a Garden Denver compressor through a 0.0508 m air line with a capacity of 1050 SCFM at 0.69 MPa. The air flow rate was measured by a Micro Motion^{TM} DL 200 mass flow rate meter. Water was pumped from the water tank by a progressive cavity pump and measured by a Micro Motion^{TM} DS 150 mass flow meter. Both liquid and gas mass flow meters were connected to a PID controller to control the mass flow rate. The measurement and control of the instruments

were automated with Labview™ data acquisition system. All of the tests were conducted under atmospheric pressure and temperature conditions.

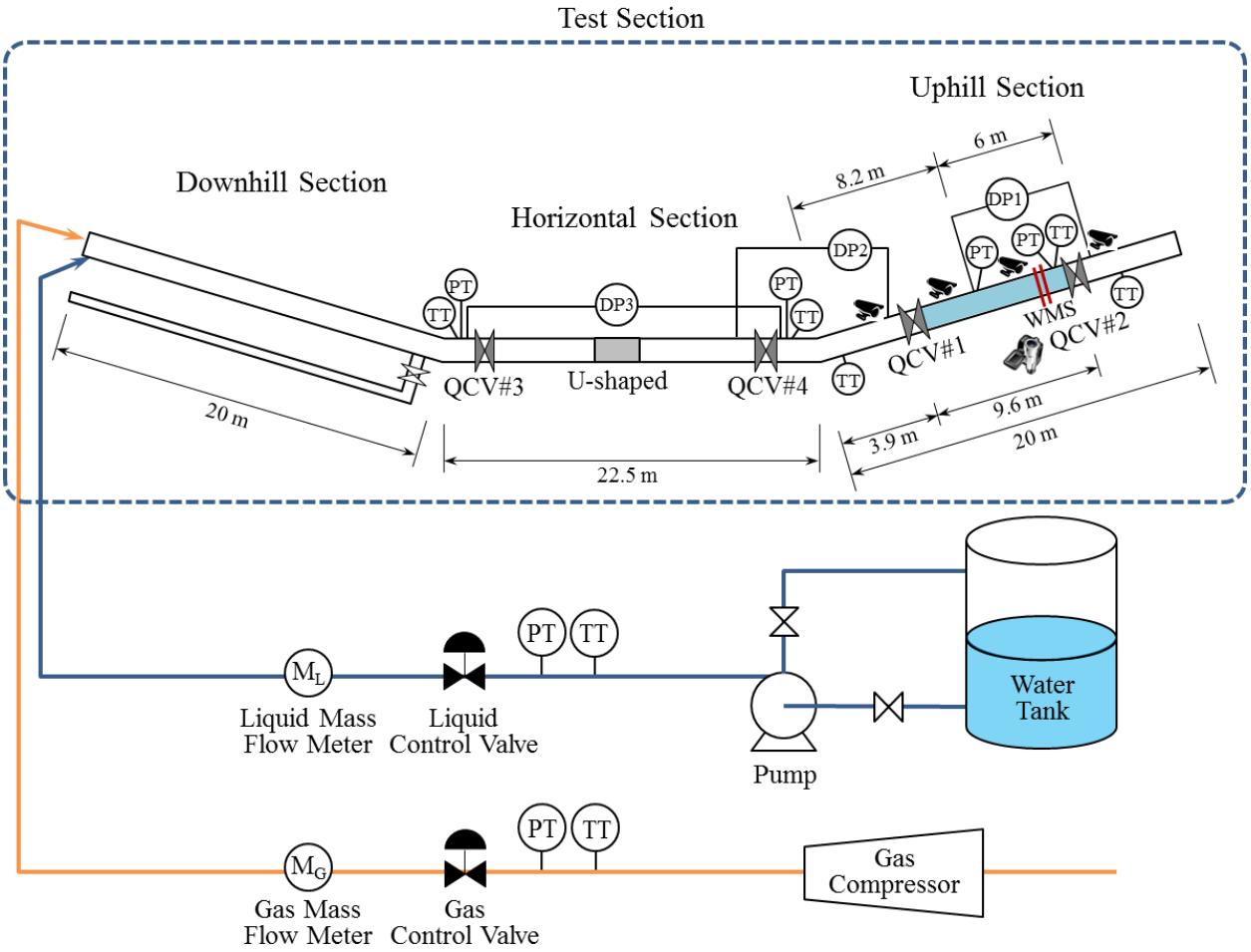

Fig. 1. Schematic of Facility (TT: Temperature Transmitter; PT: Pressure Transmitter; DP: Differential Pressure Transducer; QCV: Quick Closing Valve; WMS: Wire-mesh Sensor)

The valley configuration of the test section consisted of downhill, horizontal and uphill sections, as shown in Fig. 1. The horizontal and uphill sections were made of acrylic glass for better visualization. The outlet of the pipe was open to the atmosphere. As a result, there were no back pressure or syphon effects on the flow in the test section. The downhill section was mounted on the same boom structure as the uphill section, making the inclination angles always the same but with opposite sign. A U-shaped acrylic pipe was utilized at the middle of the horizontal section. The instrumentation of the valley test section and the corresponding dimensions are shown in Fig. 1. Overall, there were three differential pressure transducers, located in horizontal, horizontal-uphill elbow and uphill section, respectively. Three liquid holdups were measured for each test point, including H_{L1} (uphill section, between QCV#1 and QCV#2), H_{L2} (horizontal-uphill elbow, between QCV#4 and QCV#1) and H_{L3} (horizontal section, between QCV#3 and QCV#4). The current study mainly presents the pressure gradient and liquid holdup in the uphill section (dp/dL_1 and H_{L1}). There were four surveillance cameras located along the uphill section for flow pattern observation.

Wire-mesh sensors were employed in the current study to study the complex behavior of pseudo-slug flow. The experimental study was conducted in two phases. Pressure gradient and liquid holdup were measured during the first phase without wire-mesh sensor while the second phase focused only on wire-mesh sensor data acquisition. Dye injection system was employed in the first phase to study the onset of liquid film reversal.

The experimental test matrix of the current study is given in Table 1. Five inclination angles, θ, were studied while superficial liquid velocity varied from 0.001 to 0.01 m/s. Superficial gas velocity was reduced approximately from 32 m/s to 2 m/s with a step of 0.5 m/s near the onset of liquid accumulation region.

Table 1. Experimental Test Matrix for Current Study

Operating Parameters	**Range**
Pipe Geometry	Valley Test Section
Water superficial velocity, v_{SL}	0.001, 0.005 and 0.01 m/s
Air superficial velocity, v_{Sg}	32 to 2 m/s
Inclination angle, θ	2°, 5°, 10°, 15°, 20°
Operating pressure	0.1 MPa

2.1 Liquid Film Reversal Measurement

Previous experimental studies showed that liquid film reversal was the main source for liquid accumulation (Zabaras *et al*., 1986; Guner, 2012, 2015; Alsaadi, 2013, 2015; and Brito, 2015, 2016).

A special dye injection system was employed in the current study to detect the flow direction of the liquid film at pipe bottom for inclined pipe. The detailed description of the dye injection system can be found in Fan *et al*. (2018). If there is no liquid film reversal, the dye flows upward with the liquid film without any disturbance of the upstream liquid film. Once the liquid film starts to reverse, the blue dye clearly contaminates the upstream liquid film. The experimental results are presented in the next section.

2.2 Wire-mesh sensor

Since the pseudo-slug body shows a very frothy structure as compared with regular slug body, the traditional measurement techniques for slug flow, such as conductivity probe or capacitance sensor, are not reliable in term of precise measurement of the characteristics parameters. A pair of conductivity wire-mesh sensors (WMS), constructed and supported by HZDR Dresden from Germany, was employed in this study to better quantify the pseudo-slug characteristics.

WMS enables the investigation of the liquid phase distribution across the cross-sectional area of the pipe with a very high spatial and temporal resolution (Prasser *et al*., 1998). The schematic of the valley test section with WMSs is shown in Fig. 2. Also shown is a picture of WMS used in the current study.

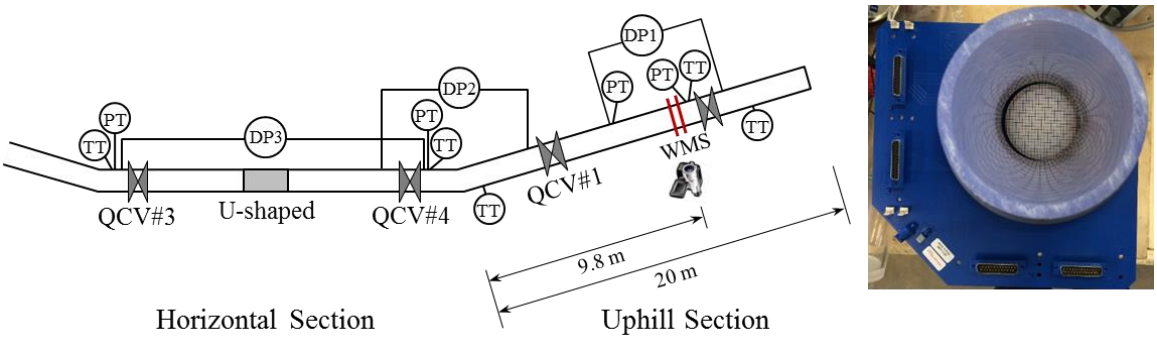

Fig. 2. Wire-mesh Sensor installation position in test section (left) and photograph (right)

The WMS measurement principle is based on a local measurement of electrical conductance of the fluid within the cross-section of a pipe by means of a mesh of crossing electrodes. Each WMS has two planes, the emitter electrodes in the first plane provide bipolar constant voltage pulses and the electrodes of the other plane arranged orthogonal to the emitter plane electrodes serve as the current receivers. There is a tiny gap of few millimeters between the emitter and receiver electrodes, where the conductance of the fluids is measured in the crossing points of the electrodes as the quotient of the received current and the supplied voltage. The wires are connected with corresponding transmitting or receiving modules, the maximum connectable transmitting electrodes of which is 16. A 24x24 WMS was specifically designed for the current study. The transmitter electrodes are activated sequentially while the receiver electrodes are sampled in parallel (Kipping *et al*., 2016). The small receiver current is amplified and converted to a voltage by means of trans-impedance amplifier circuits and eventually converted to a digital signal that is transferred to the measurement PC by means of a fast digital signal processing electronics.

As the conductance of the fluid varies with temperature, the WMSs were calibrated by fully filling the pipe with water twice each day, in the morning and afternoon, in order to minimize the temperature effect on the measurement. The final converted output of the WMS is a 3-D void fraction, ε (i, j, n), where i and j represent the coordinates across the cross-sectional area of the pipe and n refers to the frame number.

For the current study, the WMS measurement frequency was set to 5 kHz. Considering the low pseudo-slug frequency, each measurement was recorded for 300 s. The distance between the two WMSs was 0.06 m. The first sensor, the one close to inlet, was used for detailed data analysis of liquid/gas holdup distributions while the second one was utilized for the purpose of velocity measurement only.

3. Flow Pattern Classification

It is commonly recognized that in segregated flow the gas and liquid are transported separately in a stable manner; while in intermittent flow gas and liquid are transported alternately. Generally, segregate flow is consisted of stratified (ST) and annular (AN) flow, while intermittent flow includes slug (SL) and elongated-bubble (EB) flows (Shoham, 2006). It is widely accepted that slug flow is characterized by alternating flow of gas pocket and liquid slugs, in which the liquid slug body fully bocks the entire cross-sectional area of the pipe.

The transition region between segregated and regular slug flows has been widely recognized and named differently by various authors. This flow pattern has been classified as pseudo-slug whose nature is not well understood as referred in previous studies (Lin and Hanratty, 1987a, b).

In the current study, pseudo-slug flow has been classified into intermittent flow due to its intermittent nature as compared with segregated flow.

An example of the observed flow pattern map is given in Fig. 3 in a coordinate of inclination angle versus superficial gas velocity for a constant liquid flow rate. In general, the flow pattern can be classified into three categories: segregated (SEG), intermittent (INT) and the transition between segregated and intermittent flow (TRA). These flow patterns are further divided into several sub-categories based on the liquid film reversal, liquid entrainment in gas core, and the flow characteristic. Detailed description is provided in the following sub-sections.

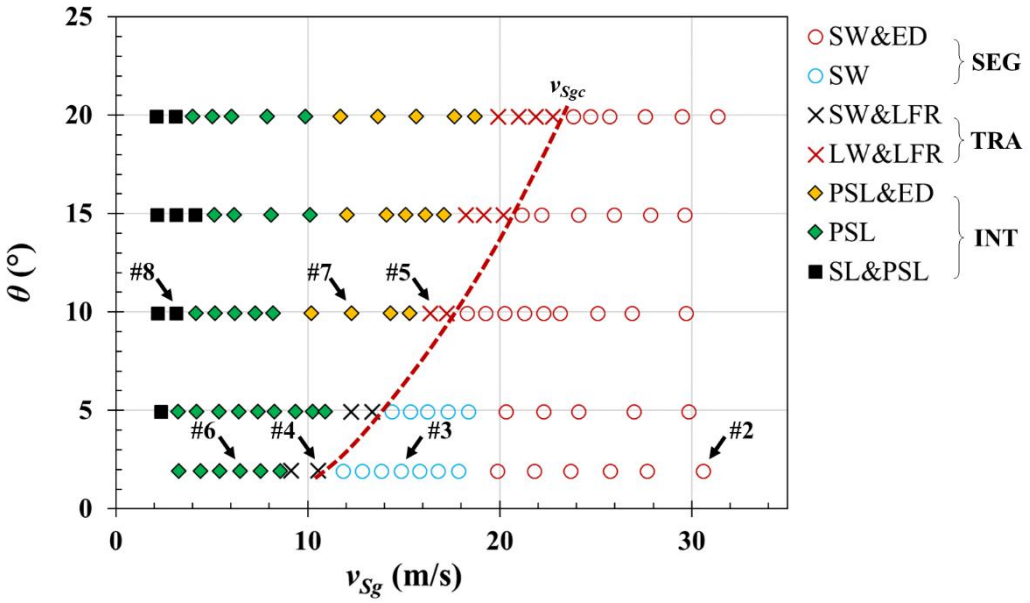

Fig. 3. Flow Pattern Map (v_{SL} = 0.005 m/s)
(SEG: Segregated flow with no film reversal; INT: Intermittent Flow; TRA: Transition between SEG and INT; SW&ED: Stratified wavy with entrained liquid droplet in gas core; SW: Stratified wavy with no liquid droplet entrainment; SW&LFR: stratified wavy with liquid film reversal at pipe bottom; LW&LFR: Large wave with liquid film reversal; PSL&ED: Pseudo-slug flow with entrained liquid droplet in film region; PSL: pseudo-slug flow with no liquid entrainment in the film region; SL&PSL: combination of slug and pseudo-slug flow)

3.1 Flow Pattern Transition between SEG, TRA and INT

The red-dash line in Fig. 3 represents the onset of liquid film reversal. To the left of the curve, the liquid phase starts to accumulate at the bottom of inclined pipe, increasing the risk of pipeline internal corrosion, and increasing pressure losses. The superficial gas velocity corresponding to the onset of liquid film reversal at pipe bottom is referred as critical gas velocity, v_{Sgc} (Fan *et al.*, 2018). In the current study, the onset of liquid film reversal is measured by a dye injection system at the bottom of inclined pipe, as shown in Fig. 4. The blue dye can easily contaminate the upstream liquid film if there is any film reversal at the bottom. Theoretically, the liquid film reversal is caused by the insufficient interfacial shear stress exposed at the gas liquid interface, which cannot overcome the gravity force exerted on the liquid film region. Detailed analysis and the corresponding mechanics model for the onset of liquid film reversal can be found in Fan *et al*.

(2018). In the current study, the onset of liquid film reversal is used as the transition from segregated flow to the other flow patterns on the left.

(a). v_{Sg} = 11.3 m/s (b). v_{Sg} = 10.2 m/s

Fig. 4. Flow Direction Test with Dye in Upward Inclined Pipe (v_{SL} = 0.005 m/s; θ = 2°)

The flow pattern transition to INT flow can be seen from the pressure gradient and liquid holdup measurement, as presented in Fig. 5. Before the onset of liquid film reversal, both phases flow separately and the frictional pressure loss dominates. The pressure gradient decreases with decreasing gas velocity due to the decreasing frictional loss in the gas phase. Once the liquid starts accumulating in the inclined pipe, the decrease of frictional pressure gradient is balanced by the increase of gravitational pressure gradient due to the increase of liquid holdup. The flow changes from frictional to gravitational dominated, and the variation of the total pressure gradient with decreasing superficial gas velocity changes from decrease to increase. After the flow changes to INT where regular periodical behavior persists, the variation of pressure gradient and liquid holdup with superficial gas velocity becomes smoother.

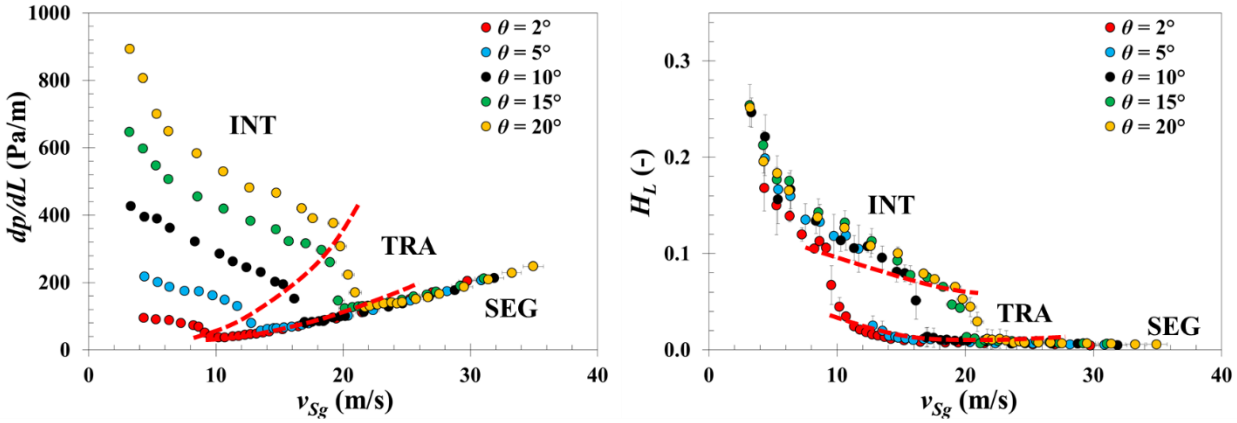

(a). Pressure Gradient vs. v_{Sg} (b). Liquid Holdup vs. v_{Sg}

Fig. 5. Variation of Pressure Gradient and Liquid Holdup with Inclination Angle and v_{Sg} at v_{SL} = 0.005 m/s

3.2 Flow Pattern Description

As aforementioned, the three major flow patterns are divided into smaller groups depending on the flow characteristics, which are described below.

3.2.1 Segregated Flow

Segregated flow occurs when the interfacial shear stress is sufficient to drag the liquid phase in the same direction as the gas phase. This flow pattern was observed at high gas flow rates (RHS of the red lines in Fig. 3).

Based on the liquid wetted perimeter and liquid entrainment, the segregated flow is subdivided into annular flow (AN), stratified wavy flow with entrained droplet (SW&ED) and stratified wavy flow without entrained liquid droplet (SW). Annular flow was only observed at v_{SL} = 0.01 m/s at high superficial gas velocities, which is shown in the flow pattern map in Appendix A. The schematics and the corresponding pictures are shown in Fig. 6, with the numbering marked in Fig. 3 and Fig. A-2. Stratified smooth flow (SS), which was observed in horizontal and near-horizontal pipe (Taitel and Dukler 1976 and Fan 2005), was not observed in the uphill section in the current study.

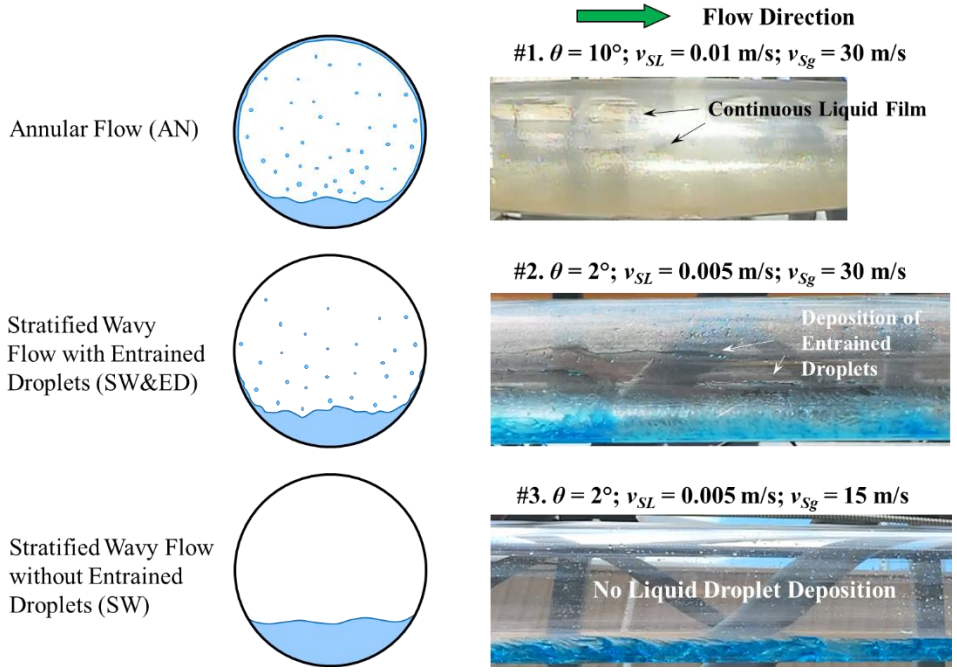

Fig. 6. Schematics and Pictures of the Sub-classified Flow Pattern in Segregated Flow

In annular flow, the gas phase flows as a core with entrained liquid droplets, while most of the liquid phase stays at the pipe bottom due to gravity. There is a continuous thin liquid film around the pipe wall, which mainly comes from the deposition of entrained liquid droplets.

When the liquid or gas flow rate is not high enough, the deposition of the liquid entrainment is not sufficient to form a continuous moving liquid film around the entire pipe wall. This flow pattern is called stratified flow (Shoham, 2006). Based on the liquid entrainment, the stratified flow is sub-divided into stratified wavy flow with entrained droplet (SW&ED) and without entrained droplet (SW). For SW&ED, the entrained liquid droplets have been observed hitting the pipe wall intermittently due to the high turbulence of the gas core, as illustrated in Fig. 6. As a comparison, there is no liquid droplet deposition observed for SW. SW occurs at lower liquid and gas flow rates as compared with SW&ED.

3.2.2 Transition Region

When the interfacial shear stress is not enough to drag all of the liquid in the film in upward direction, the liquid flow direction at the bottom of the pipe reverses due to gravity as described

in Section 3.1. In the current study, the flow pattern, which occurs after the onset of liquid film reversal but does not show clear regular intermittent behavior as pseudo-slug/slug flow does, is named as transition region (TRA). Based on the liquid entrainment and wave behavior at the interface, this flow pattern is sub-divided into two categories, the pictures of which are shown in Fig. 7.

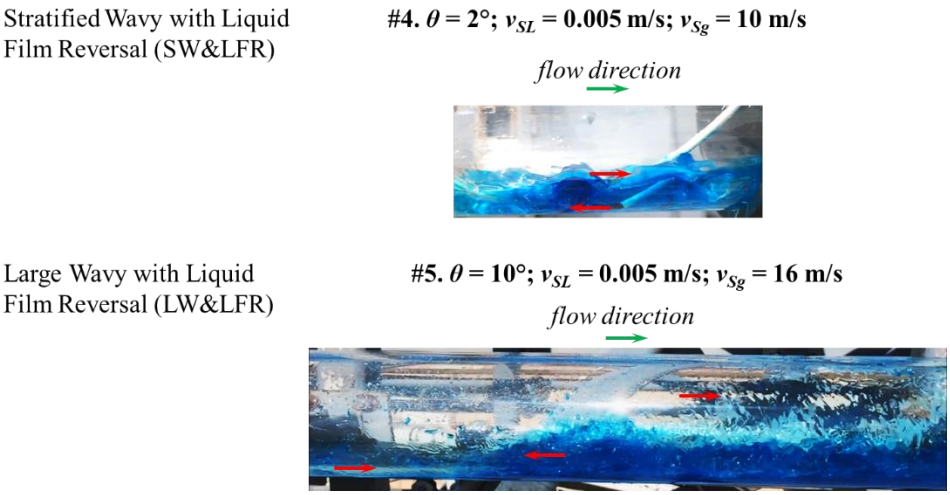

Fig. 7. Pictures of the Sub-classified Flow Pattern in Transition Region

For low inclination angles (2° and 5° in the current study), this transition region is simply stratified wavy with liquid film reversal (SW&LFR). Roll waves were observed at the gas liquid interface (Fig. 7). This flow pattern is marked as black crosses in Fig. 3.

For higher inclination angles (10°, 15° and 20° in the current study), large backward flowing waves were observed as shown in Fig. 7. The gas phase breaks the large waves and creates a large amount of liquid droplets, which are entrained in the gas phase. The entrained liquid droplets then deposit on the pipe wall generating a liquid film surrounding the pipe wall. The flow behavior is chaotic and shows no significant intermittent behavior as compared with intermittent flow. The difference between the transition region and intermittent flow can also be reflected from the pressure gradient and liquid holdup data as shown before in Fig. 5. This flow pattern is also different from regular annular flow in that the large liquid waves move backward. This flow pattern is named as large wave with liquid film reversal (LW&LFR) in the current study, which is marked as red crosses in Fig. 3.

The transition region is very narrow as compared with other well-defined flow patterns, such as segregated, pseudo-slug (explained later), or slug flow. It may not attract too much attention from modeling point of view, but it serves as a bridge between segregated and intermittent flow.

3.2.3 Intermittent Flow

With decreasing v_{Sg}, the intermittent behavior of the liquid phase is more evident, similar with slug flow but with a frothy liquid body. This flow pattern has been classified as pseudo-slug flow (PSL). The current study sub-divides the pseudo-slug flow pattern into two sub-classifications depending on the liquid entrainment in the film region. The flow patterns are pseudo-slug flow with entrained liquid droplet in the film region (PSL&ED), and pseudo-slug

flow with no entrainment in the film region (PSL). The corresponding pictures are shown in Fig. 8.

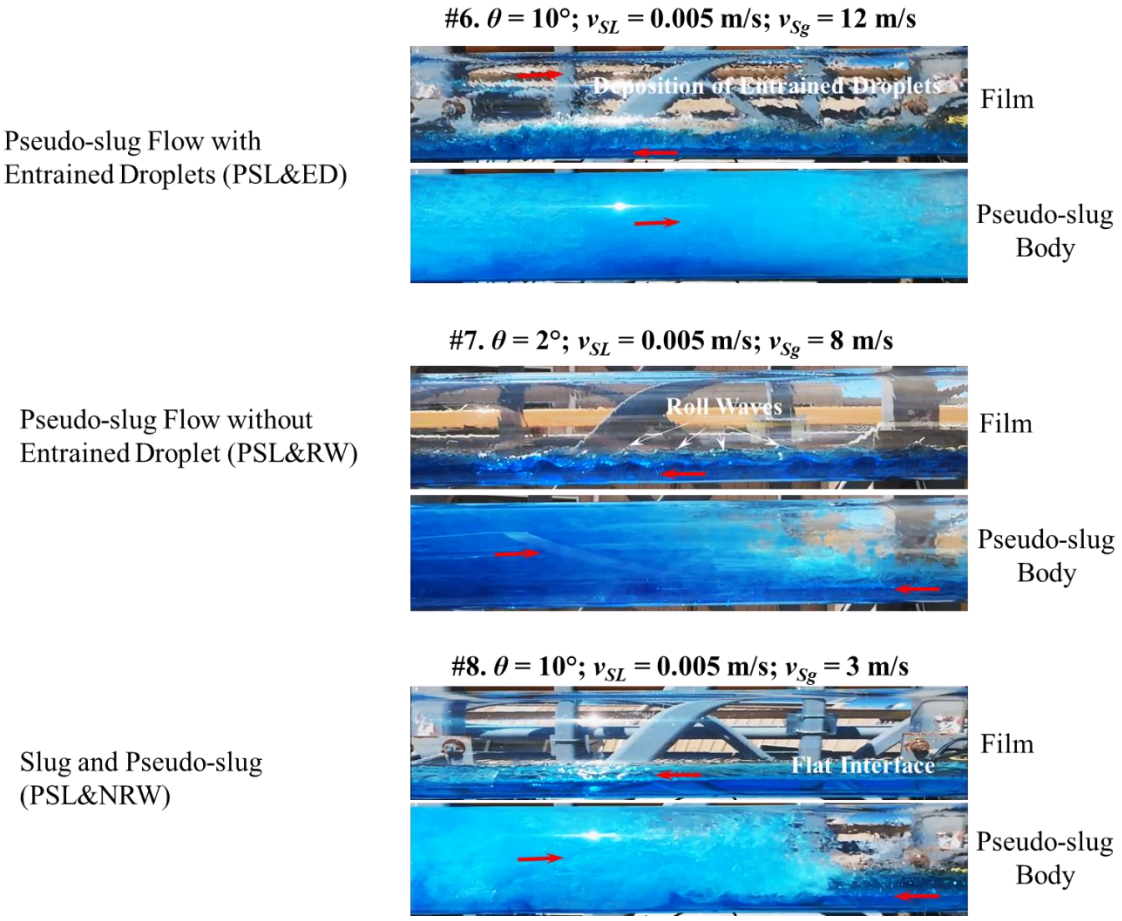

Fig. 8. Pictures of the Sub-classified Flow Pattern in Pseudo-slug Flow

PSL&ED is marked as orange diamond in Fig. 3. At the gas/liquid interface in the film region, the gas phase breaks the roll waves and entrains the created liquid droplets into the gas phase. The deposition of the entrained liquid droplets then forms a thin liquid film surrounding the pipe wall as shown in Fig. 8 (#6). For this flow pattern, the liquid phase is transported by three flow structures: pseudo-slugs, liquid film and liquid droplets entrained in the gas phase in the film region, the amount of which depends on inclination angle and the gas flow rate. This flow pattern was observed at high inclination angles ($\theta \geq 10°$) and high superficial gas velocities.

For lower inclination angles (2° and 5° in the current study), the gas phase is unable to break the waves due to the higher gravitational force perpendicular to the liquid film. Consequently, there is no entrained liquid droplet observed in the liquid film region. For high superficial gas velocities, roll waves are still observed at the interface as shown in Fig. 8 (#7). At lower superficial gas velocities, smooth interface or backward flowing tiny ripple waves were observed at the gas/liquid interface in the liquid film region (#8 in Fig. 8).

A graduate and smooth transition from pseudo-slug to conventional slug flow was observed at the lowest gas flow rates. The flow pattern, which includes both pseudo-slug and slug flows,

is named as Slug&Pseudo-slug (SL&PSL). A detailed description of the comparison between conventional slug and pseudo-slug is provided in the next section, followed by the transition between PSL and PSL&SL.

3.3 Comparison between pseudo-slug and slug

Figure 9 shows pictures of a slug (left) and a pseudo-slug (right) respectively. It can be seen in Fig. 9 (a) that the liquid phase within the slug body can fully block the entire cross-sectional area of the pipe with some gas bubbles entrained in the slug body. However, the pseudo-slug body shows a much more frothy structure as compared with slug flow as shown in Fig. 3 (b).

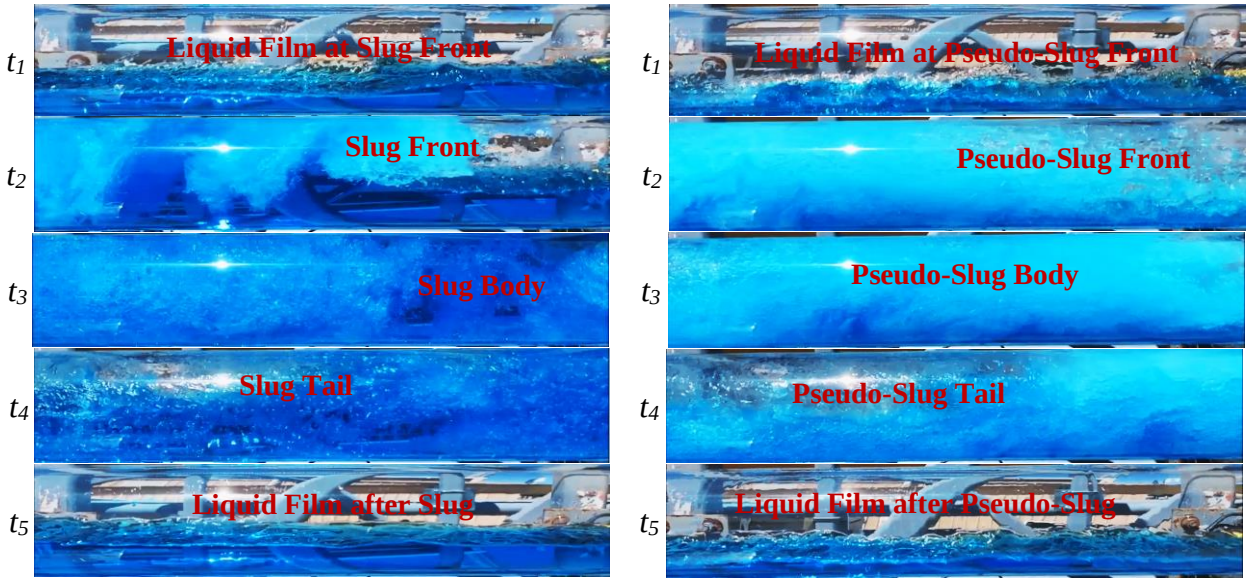

(a). Slug
(θ = 10°; v_{SL} = 0.005 m/s; v_{Sg} = 3 m/s)

(b). Pseudo-slug
(θ = 10°; v_{SL} = 0.005 m/s; v_{Sg} = 6 m/s)

Fig. 9. Images of Regular Slug (a) and Pseudo-slug (b)

To better understand the liquid phase distribution within pseudo-slug body, wire-mesh sensor data were analyzed from different perspectives. Figures 10 and 11 show examples of a slug body and pseudo-slug body, respectively. The 3-D plots on top illustrate the iso-surface evolution for slug and pseudo-slug flows. The iso-surfaces were generated by Tecplot^{TM} by connecting the points having the same liquid holdup (0.3 for the current study) within the volumetric data field (Tecplot 360^{TM} User's Manual Version 2013). The 2-D axially sliced images in Figs. 10 and 11 show the liquid holdup distribution evolution at the center of the cross-sectional area of the pipe, while the figures at bottom illustrate the spontaneous liquid phase distribution at the pipe cross-sectional area at different time.

Figure 10 shows clearly that, the liquid phase can fully block the entire cross-sectional area of the pipe in slug liquid body. The 3-D images also illustrate the entrained gas bubbles within the continuous liquid phase in slug body. Since the passage of the continuous gas phase is fully blocked by the continuous liquid slug body, the slug body is pushed forward by the upstream gas pocket efficiently, leading to a greater slug translational velocity than the mixture velocity. The translational velocity of this particular slug is 3.9 m/s, which is comparable with that calculated

from slug translational velocity closure relationship (3.6 m/s from Nicklin *et al*. (1964) with v_D from Bendiksen (1984), and 1.2 as the flow coefficient).

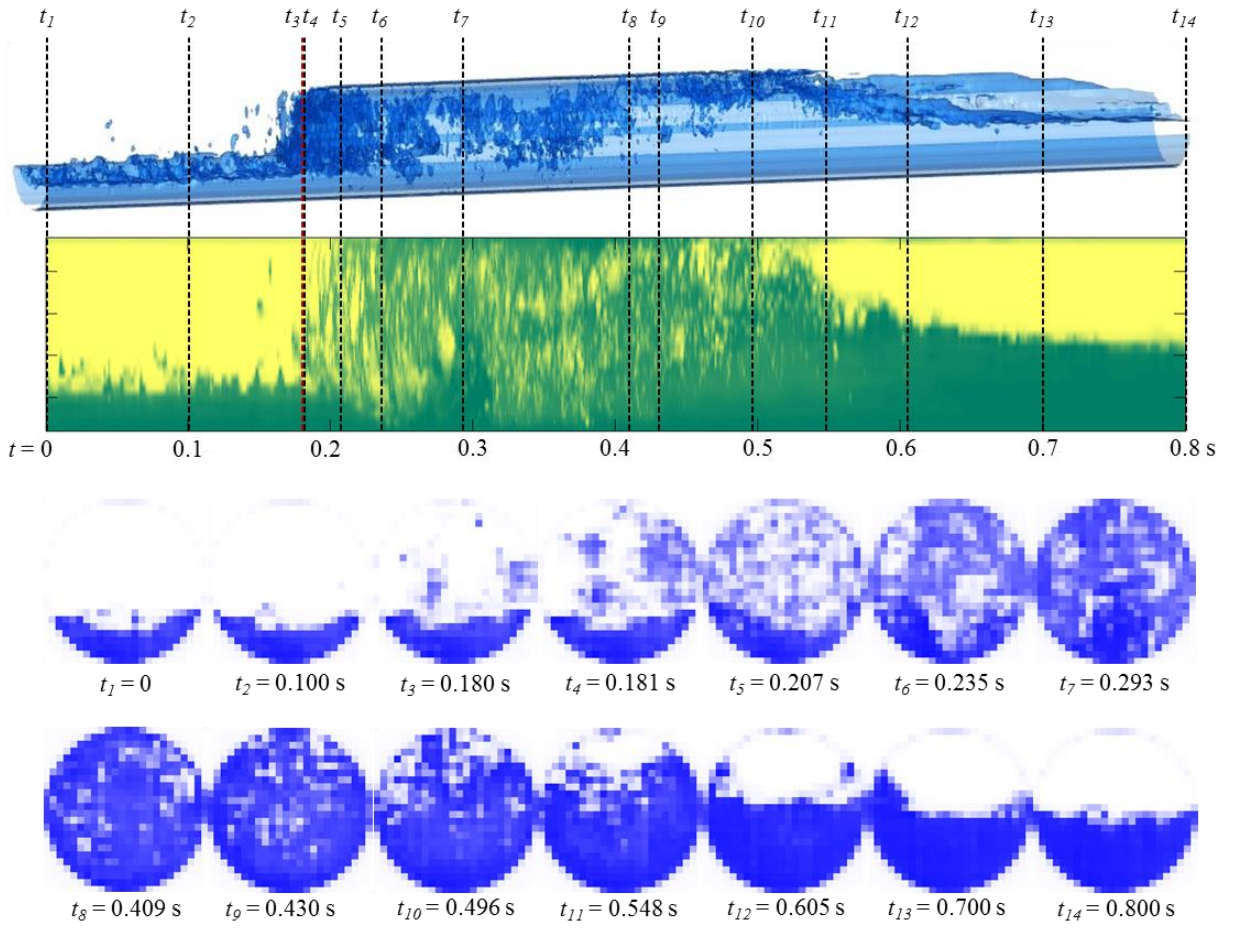

Fig. 10. WMS Data Visualization of a Slug Body (θ = 10°; v_{SL} = 0.005 m/s; v_{Sg} = 2.6 m/s; v_T = 3.9 m/s) (Top: iso-surface created by Tecplot™ 360; Middle: liquid holdup evolution at pipe center; Bottom: liquid phase distribution at different time)

However, the pseudo-slug body shows a different topological structure within the body as shown in Fig. 11. It can be seen that the liquid phase cannot fully block the entire cross-sectional area of the pipe in the pseudo-slug body, consequently there is continuous gas flowing through the pseudo-slug body. It has also been observed that there is a large amount of liquid droplet entrained in the gas phase passing through the pseudo-slug body. The deposition of these droplets forms a liquid film surrounding the pipe wall (t_5 – t_{10} in Fig. 11). The translational velocity of this particular pseudo-slug is 2.54 m/s, much less than the gas superficial velocity, 6.1 m/s. This observation is consistent with the findings from previous literatures (Lin and Hanratty, 1987a; Ekinci, 2015; Fan *et al*., 2015; and Fan, 2017).

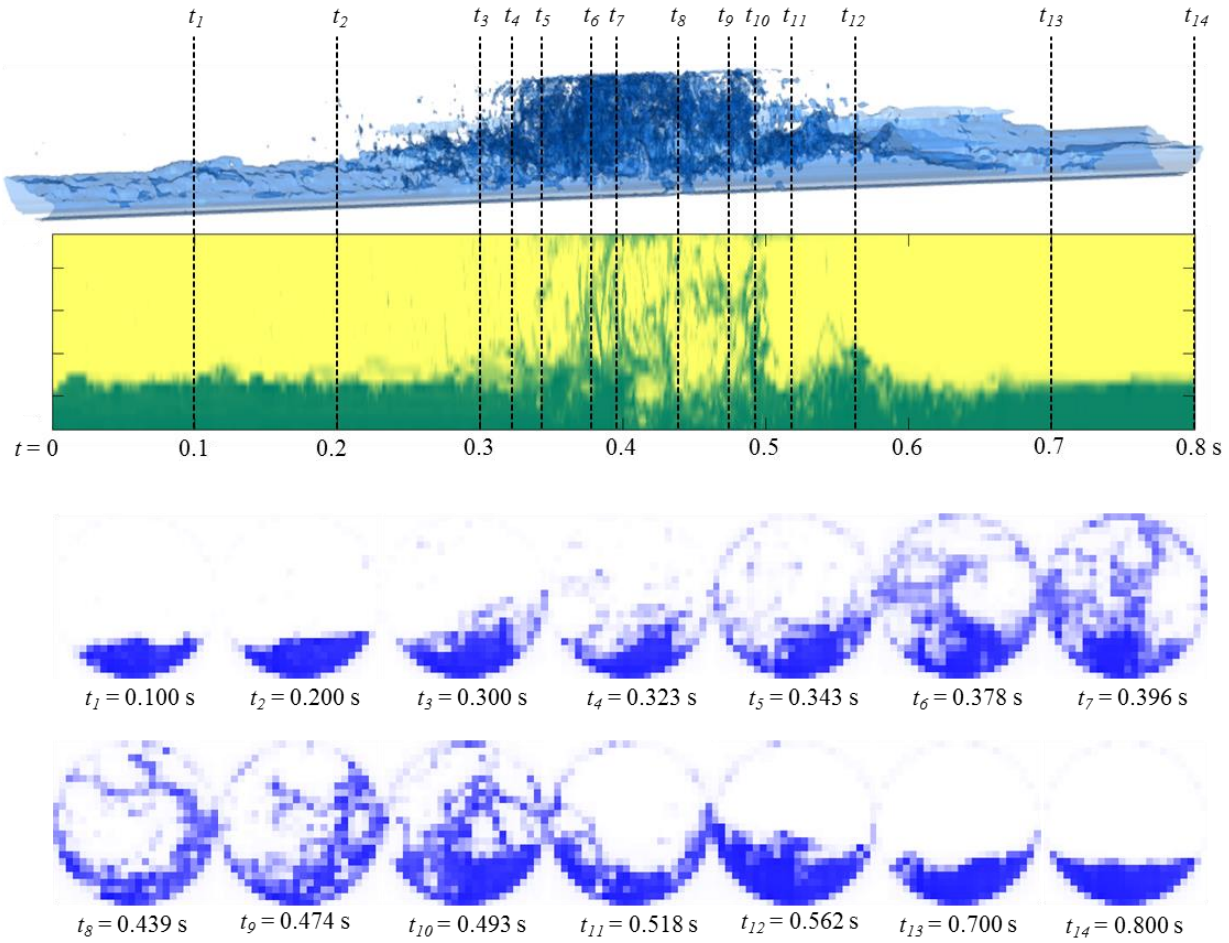

Fig. 11. WMS Data Visualization of a Pseudo-slug Body (θ = 10°; v_{SL} = 0.005 m/s; v_{Sg} = 6.4 m/s; v_{PSL} = 2.54 m/s) (Top: iso-surface created by Tecplot^{TM} 360; Middle: liquid holdup evolution at pipe center; Bottom: liquid phase distribution at different time)

3.4 Transition from PSL to SL

As aforementioned, there is no sudden change from pseudo-slug to conventional slug flow. There is a region in which both pseudo-slug and conventional slug coexist, the number fraction of which depends on the inclination angle, gas and liquid flow rates, fluid properties, etc.

To illustrate the superficial gas velocity effects on flow pattern transition, a series of 1-D average H_L data and 2-D liquid holdup distribution at pipe center are shown in Figs. 12-14 for different gas velocities (2.1, 4.1 and 6.1 m/s, respectively). The plots on top represent the variation of spatial average liquid holdup from wire-mesh sensor with time. It is worth to mention that the x-axis of the 3-D and 2-D axial images in Figs. 12 – 14 represents time, not length. The time duration of the slug/pseudo-slug body does not stand for the actual slug/pseudo-slug body length. It can be seen that the flow structure varies even at one constant superficial gas velocity. At v_{Sg} = 2.1 m/s (the lowest v_{Sg} that the current study can reach at), both slug and pseudo-slug are observed (Fig. 12), while slug flow dominates. Figure 13 shows that the flow structure gradually becomes pseudo-slugs dominated with increasing v_{Sg}. Only pseudo-slugs are observed when superficial gas velocity is increased to 6.1 m/s (Fig. 14).

Figure 15 shows the variation of the pseudo-slug and slug number fraction with gas and liquid flow rates and inclination angle. It can be seen that conventional slug starts to occur when the superficial gas velocity decreases to a critical velocity, the value of which depends on inclination angle and liquid flow rate for the current experimental condition. Then, the number fraction of conventional slug body increases with decreasing gas flow rate or increasing liquid flow rate. It can be concluded from Fig. 15 that the transition from pseudo-slug to conventional slug flow does not occur abruptly. There is a smooth transition between these two flow patterns. Figure 15 also shows that the slug fraction increases with increasing inclination angle (for ≤ 20°). This trend can also be illustrated from the pseudo-slug velocity plot, as discussed below.

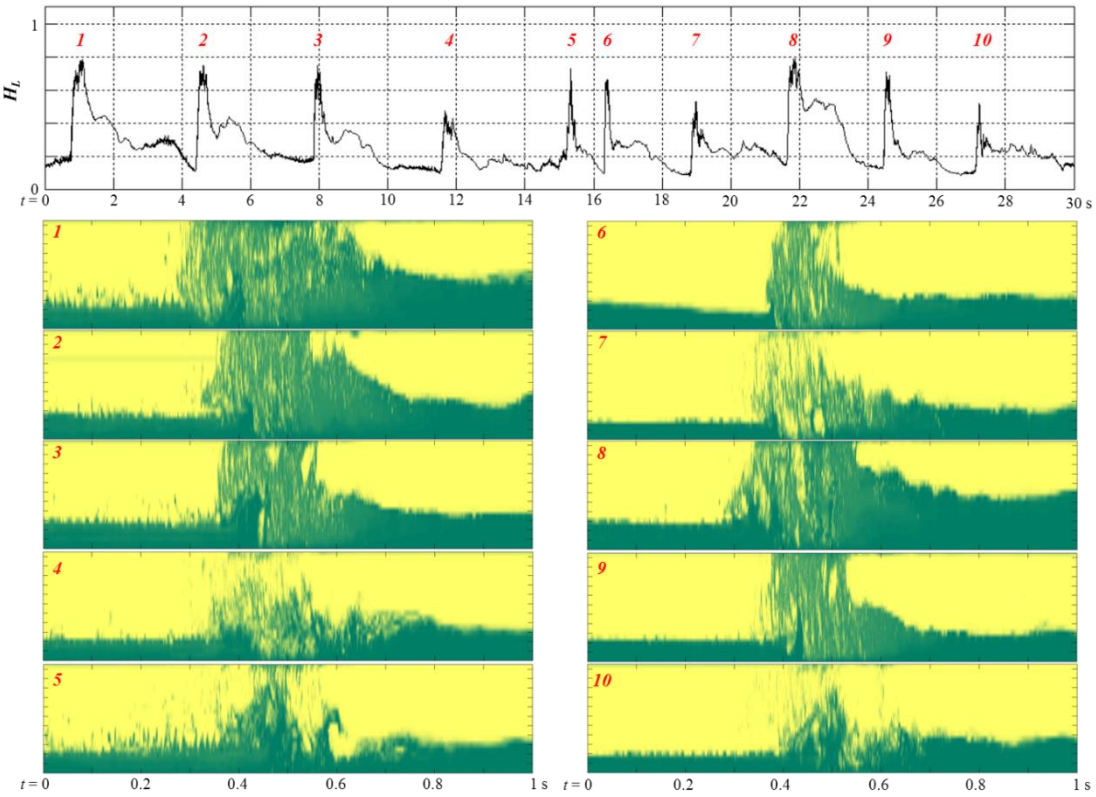

Fig. 12. 1-D and 2-D Liquid Holdup Evolution (θ = 10°; v_{SL} = 0.005 m/s; v_{Sg} = 2.1 m/s)

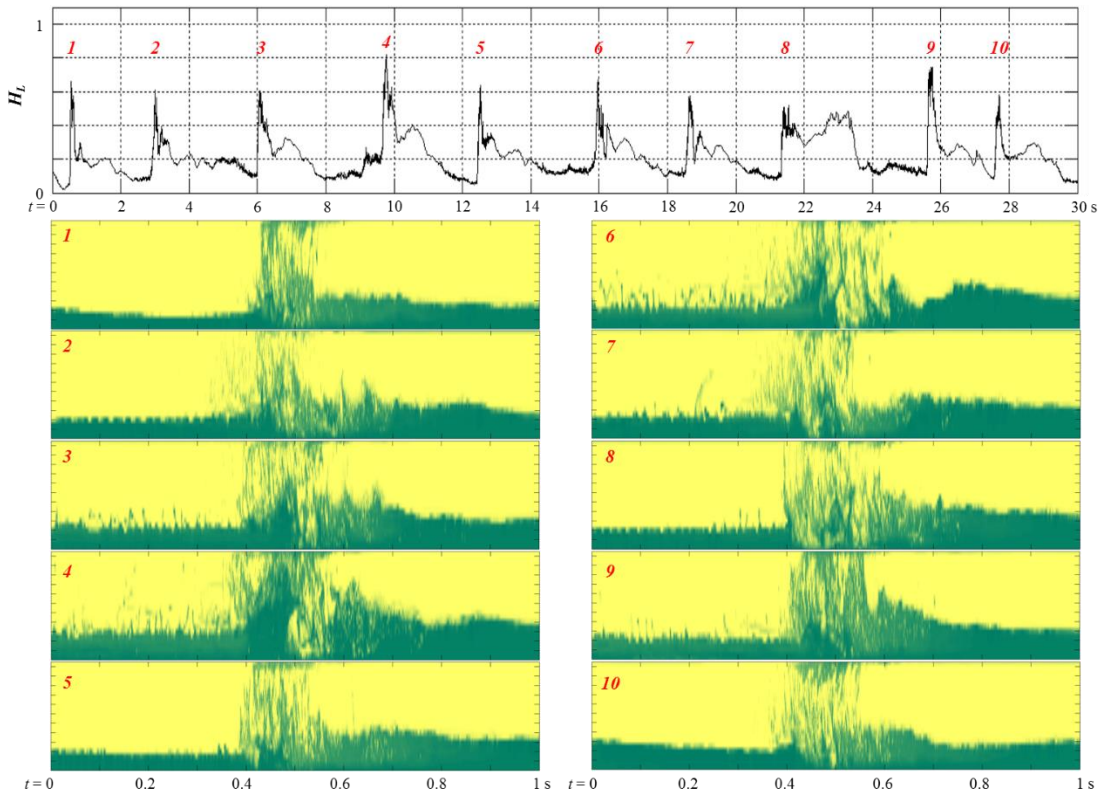

Fig. 13. 1-D and 2-D Liquid Holdup Evolution (θ = 10°; v_{SL} = 0.005 m/s; v_{Sg} = 4.1 m/s)

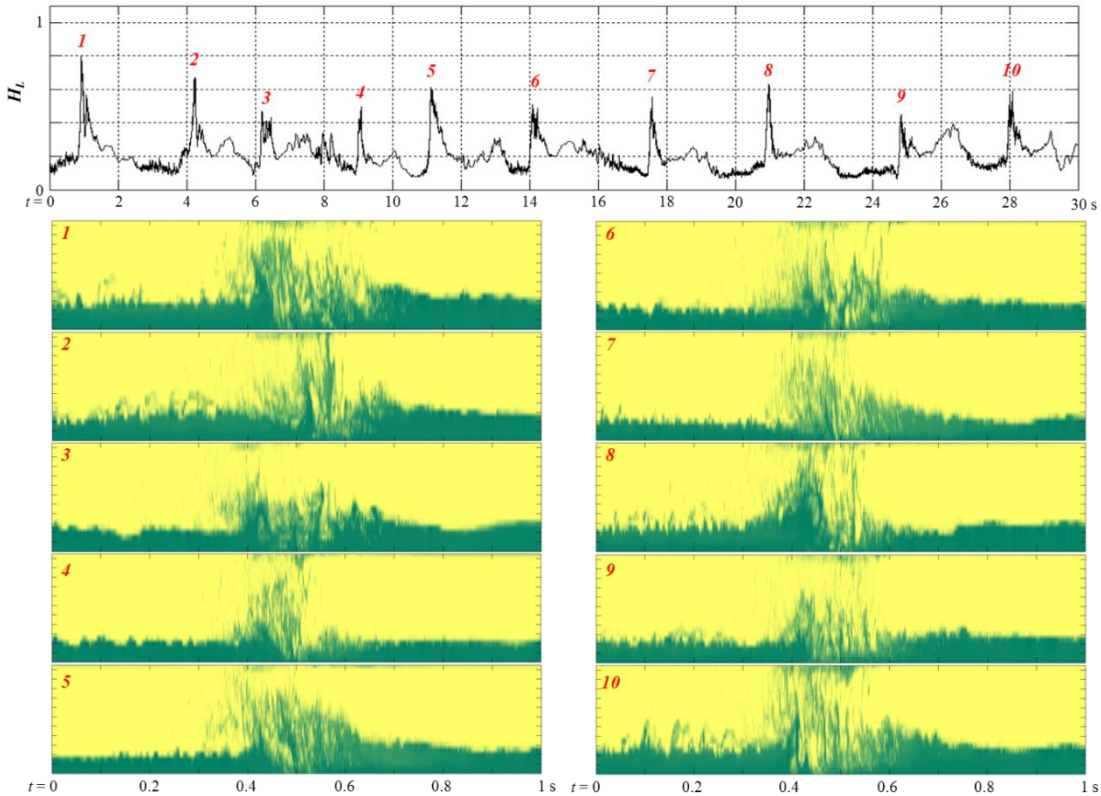

Fig. 14. 1-D and 2-D Liquid Holdup Evolution (θ = 10°; v_{SL} = 0.005 m/s; v_{Sg} = 6.1 m/s)

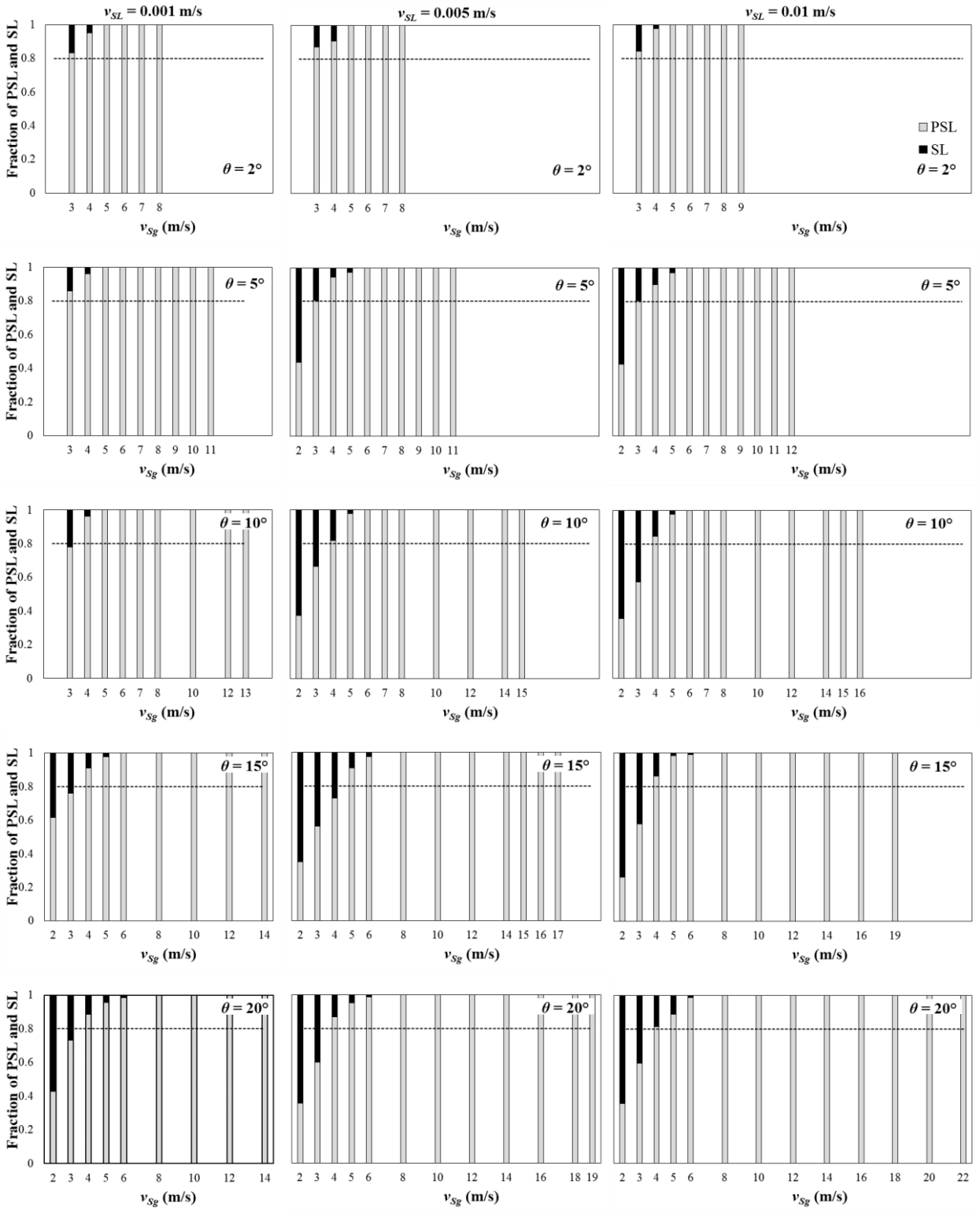

Fig. 15. Fraction of Number of Slug and Pseudo-slug over the Total Number of Structure

It has been recognized that one of the distinguished difference between conventional slug flow and pseudo-slug flow is their structure velocity (Lin and Hanratty, 1987a; Fan *et al*., 2015;

Ekinci, 2015). Pseudo-slug flow shows a smaller structure velocity as compared with slug flow due to the insufficient blockage. Figure 16 shows the variation of the structure velocity with superficial gas velocity for the five different inclination angles, which also indicates the flow pattern transition. In SEG and TRA, the structure velocity represents wave celerity (C_W), which decreases with decreasing gas flow rate. When intermittent flow initiates, the structure velocity corresponds to the pseudo-slug body velocity for PSL (v_{PSL}), or slug translational velocity for SL (v_T). The blue diamond represents the slug translational velocity from Felizola (1992) for air and low-viscosity-oil pipe flow with inclination angle from 0° to 30°. The dash line in Fig. 16 represents the correlation for slug translational velocity proposed by Nicklin *et al*. (1962), as follows:

$$v_T = c_0 v_M + v_D, \tag{1}$$

where c_0 is a flow distribution coefficient that represents the mixture velocity contribution to the slug translational velocity and v_D is the drift velocity, which represents the velocity of a Taylor-Bubble in a stagnant liquid. The drift velocity proposed by Benjamin (1968) for horizontal flow was used in Fig. 16, the expression of which is shown as following:

$$v_D = 0.54\sqrt{gd}\,. \tag{2}$$

It is not new that the translational velocity follows Eqn. (1) for conventional slug flow (Ekinci, 2015; Soedarmo *et al*., 2018; Felizola, 1992). Interestingly, the pseudo-slug flow structure velocity falls in between the traditional slug translational velocity and the wave celerity. Combining with Fig. 15, it can be seen that when the fraction of number of SL is higher than 0.2, the structure velocity matches with the traditional slug translational velocity well indicating the transition from PSL dominated to SL dominated, keeping in mind that the slug body carries more liquid than pseudo-slug body. In another words, the structure velocity can be used as an indicator for the transition to PSL. When the average structure velocity deviates from Nicklin *et al*. (1962), the flow pattern becomes pseudo-slug flow. In the current study, the transition from PSL to SL&PSL occurs when the structure velocity collapses with the traditional slug translational velocity, as shown in Fig. 16.

The inclination angle effect on the structure velocity is more evident in pseudo-slug flow region. To better understand the inclination angle effect on structure velocity, the liquid phase distribution within pseudo-slug body is analyzed. Figure 17 compares the liquid phase distribution in pseudo-slug body for two different inclination angles (2° and 15°). It is speculated that the pseudo-slug body velocity is a function of the degree of mixing of gas and liquid phase in pseudo-slug body, although the liquid holdup in pseudo-slug body does not show significant difference (Fan, 2017). The liquid phase distribution at the pipe cross-sectional area in Fig. 17 shows that the gas phase tends to stay at the upper part of the pseudo-slug body for the lower inclination angle, owing to the higher gravity component perpendicular to the flow direction which facilitates separation. More mixing is observed for the higher inclination angle resulting in a more efficient blockage of the gas passage, and a higher structure velocity as a consequence. This may also relate with the transition to SL&PSL in terms of inclination angle effects as shown in Fig. 15.

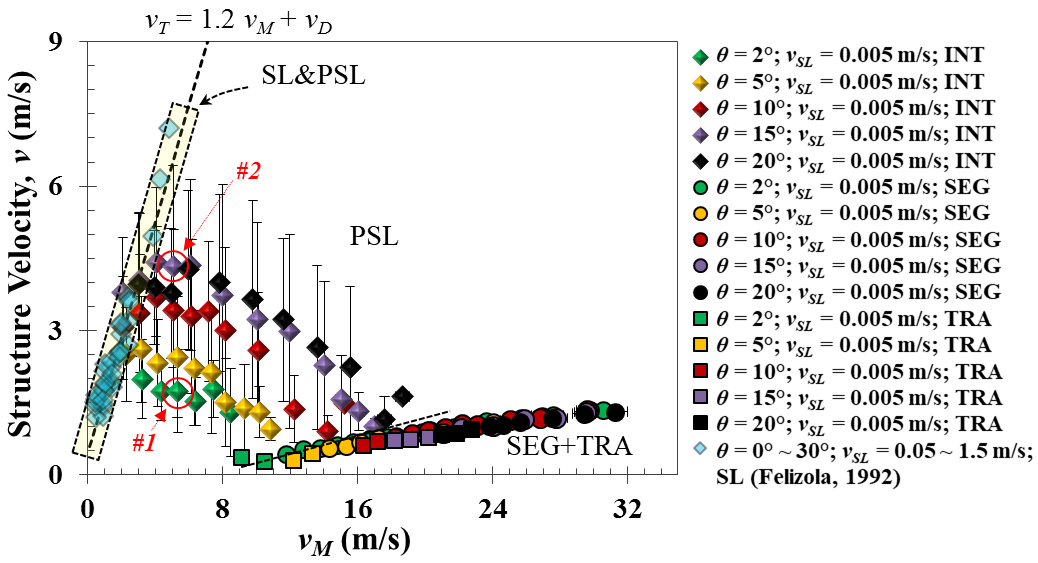

Fig. 16. Variation of Structure Velocity with Mixture Velocity and Inclination Angle

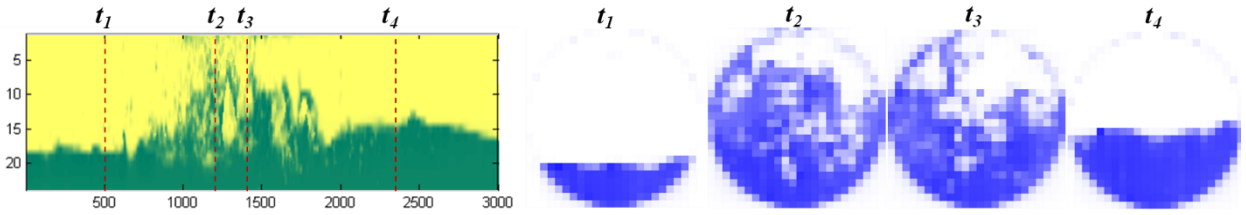

(a). θ = 2°; v_{SL} = 0.005m/s; v_{Sg} = 5.3 m/s (#1 in Fig. 16)

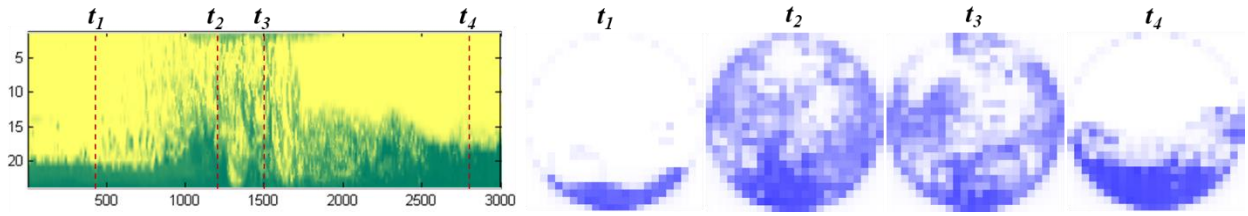

(b). θ = 15°; v_{SL} = 0.005m/s; v_{Sg} = 5.1 m/s (#2 in Fig. 16)

Fig. 17. Inclination Angle Effect on Liquid Phase Distribution in Pseudo-slug Body

4. Simple correlation for pseudo-slug structure velocity

The current experimental data shows that the structure velocity in PSL region shows a nearly "linear" relationship between v_T and C_W (Fig. 16). Based on this phenomenon, we propose two simplified approaches to estimate the pseudo-slug velocity, which can be easily implemented in any pseudo-slug point model. Since the data for pseudo-slug flow is very limited in literature, only the data from the current study was used for the development of the closure relationship.

4.1. First Approach

The first approach assumes a linear relationship between SL and SEG flow with a constant slope for all inclination angles, C_{PSL}, which can be a function of pressure, pipe diameter, liquid flow rate and fluid properties. The right boundary is combined with the wave celerity at the critical gas velocity for the onset of liquid film reversal. Based on the current experimental data, the following correlation is proposed:

$$v_{PSL} = C_{PSL}\left(v_M - v_{Sgc} - v_{SL}\right) + C_{W@v_{Sgc}}, \tag{3}$$

where v_{Sgc} is the critical gas velocity for the onset of liquid film reversal, and $C_{W@v_{Sgc}}$ is the corresponding wave celerity. In this paper, Fan *et al*. (2018) model is used to calculate the critical gas velocity; while the wave celerity is calculated from Gawas *et al*. (2014). The comparison between the measured and predicted structure velocity and the performance curve are shown in Figs. 18 – 20 for different liquid flow rates. For these cases, C_{PSL} was obtained by fitting the current experimental data. It can be seen from Figs. 18-20 that, the magnitude of the slope decreases with increasing liquid flow rate, which is mainly due to the v_{SL} effect on the right boundary (onset of liquid film reversal). However, the transition from SL&PSL to PSL is not sensitive to the liquid flow rate for the current experimental conditions.

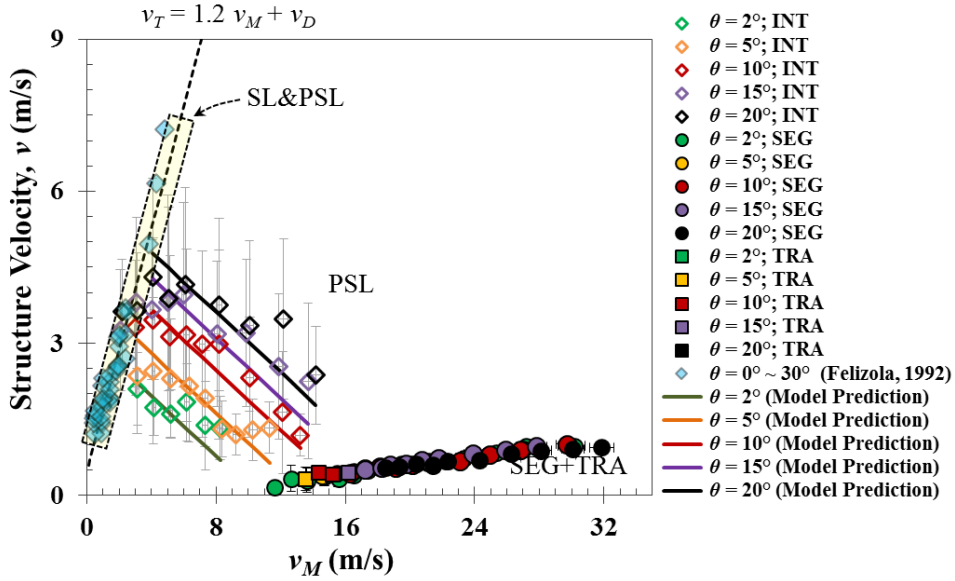

Fig. 18. Comparison between measured and predicted pseudo-slug velocity from the first approach for v_{SL} = 0.001 m/s, (C_{PSL} = -0.2962)

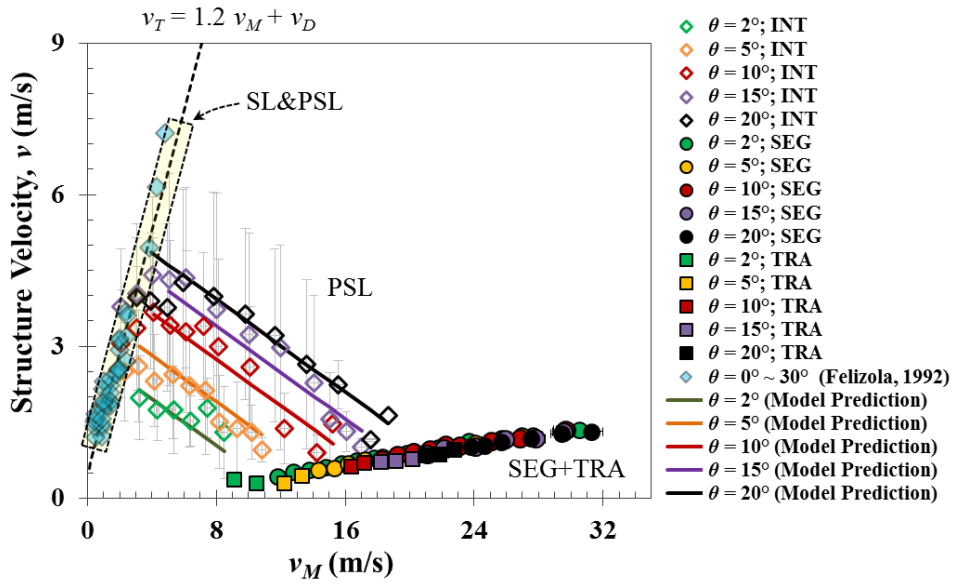

Fig. 19. Comparison between measured and predicted pseudo-slug velocity from the first approach for v_{SL} = 0.005 m/s, (C_{PSL} = -0.2297)

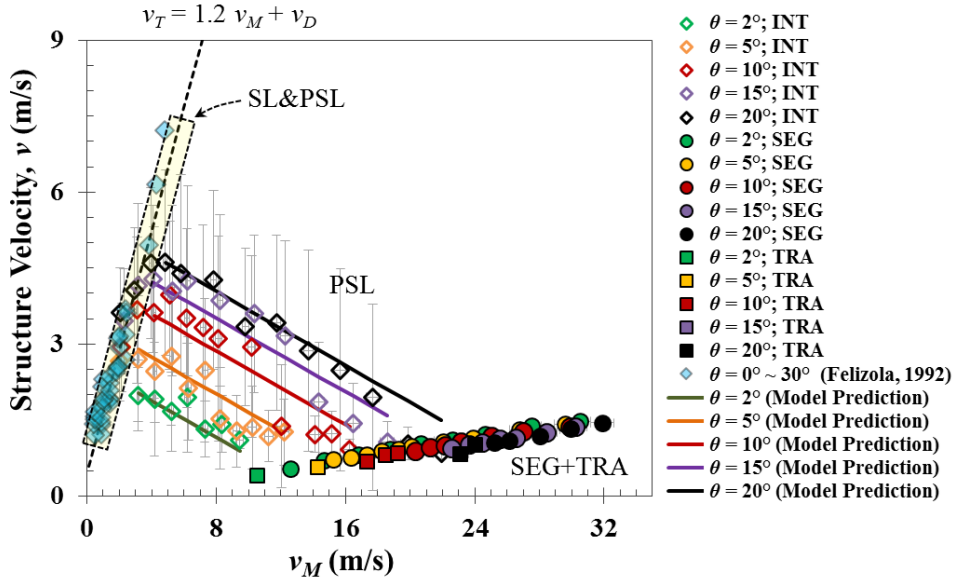

Fig. 20. Comparison between measured and predicted pseudo-slug velocity from the first approach for v_{SL} = 0.01 m/s, (C_{PSL} = -0.1820)

4.2. Second Approach

To apply the first approach, C_{PSL} has to be determined, which requires further experimental investigation. This brings the second approach, which employs the flow pattern transition from SL&PSL to PSL as the left boundary. The right boundary is still the onset of liquid accumulation, same as in the first approach. We analyzed the existing models for the SL to CH/PSL transition as reviewed by Soedarmo *et al*. (2018), showing that the wave effect of Taylor bubble concept proposed by Chen and Brill (1997) gives the best prediction of inclination angle effect on the flow pattern transition. As a result, the extension of the slug to churn

transition in upward vertical two-phase flow proposed by Chen and Brill (1997) in inclined pipe is employed as the transition boundary in the second approach. The criteria for the transition from slug to churn flow is given by:

$$L_S / L_U \le 0.15 \text{ or } H_{LS} \le 0.48, \tag{4}$$

where L_S is the slug body length, L_U is slug unit length, H_{LS} is the liquid holdup in slug body. As discussed in Section 3.4, the transition from conventional slug to pseudo-slug is gradual. From modeling point view, it is more essential to identify the transition from SL&PSL to PSL instead of SL to SL&PSL, where the structural velocity begins to show different behavior. In the current study, 0.1 was used as the criteria instead of 0.15, while the L_S and L_U was calculated from TUFFP Unified Model (Zhang *et al*., 2003). The pseudo-slug velocity, v_{PSL} can be expressed as:

$$v_{PSL} = C_{PSL} v_M - \left(v_{T@v_{Sgt}} - C_{W@v_{Sgc}} \right) \frac{v_{Sgt} + v_{SL}}{v_{Sgt} - v_{Sgc}} + v_{T@v_{Sgt}}, \tag{5}$$

where,

$$C_{PSL} = \frac{v_{T@v_{Sgt}} - C_{W@v_{Sgc}}}{v_{Sgt} - v_{Sgc}}, \tag{6}$$

$$v_{T@v_{Sgt}} = c_0 \left(v_{Sgt} + v_{SL} \right) + v_D, \tag{7}$$

$$v_D = 0.54\sqrt{gd}\cos(\theta) + 0.35\sqrt{gd}\cos(\theta). \tag{8}$$

In above equations, v_{Sgt} is the superficial gas velocity corresponding to the transition from SL&PSL to PSL from modified Chen and Brill (1997) model, and $v_{T@v_{Sgt}}$ is the corresponding slug translational velocity from Nicklin *et al*. (1962). C_0 is the flow distribution coefficient and equals to 1.2 for the current experimental condition. The drift flux velocity, v_D, is from Bendiksen *et al*. (1984) as given in Eqn. (8). θ is the pipe inclination angle from horizontal.

The comparisons of experimental data and the model predictions from the second approach are shown in Figs. 21 - 23. The red diamonds represent the model prediction for the flow pattern transition from SL&PSL to PSL, showing good agreement. It can also be seen that the second approach captures well the inclination angle and liquid flow rate effects on v_{PSL}. Another advantage of the second approach is that it links the pseudo-slug flow with conventional slug flow from the modeling point of view.

The model performance curve for the above two methods were shown in Fig. 24, while the statistical parameter is listed in Table 2. In general, both methods give fair prediction with the average absolute error less than 20%.

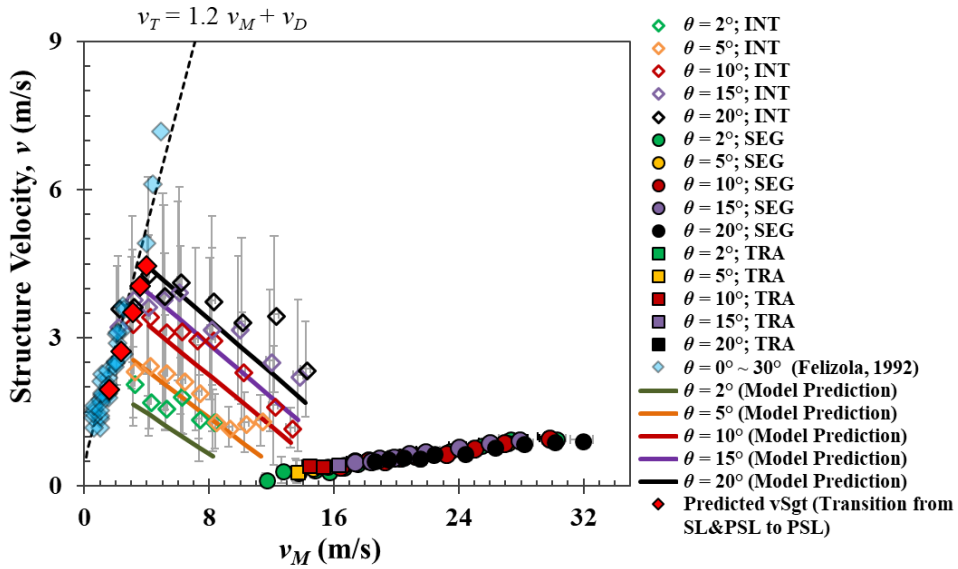

Fig. 21. Comparison between measured and predicted pseudo-slug velocity from the second approach for v_{SL} = 0.001 m/s

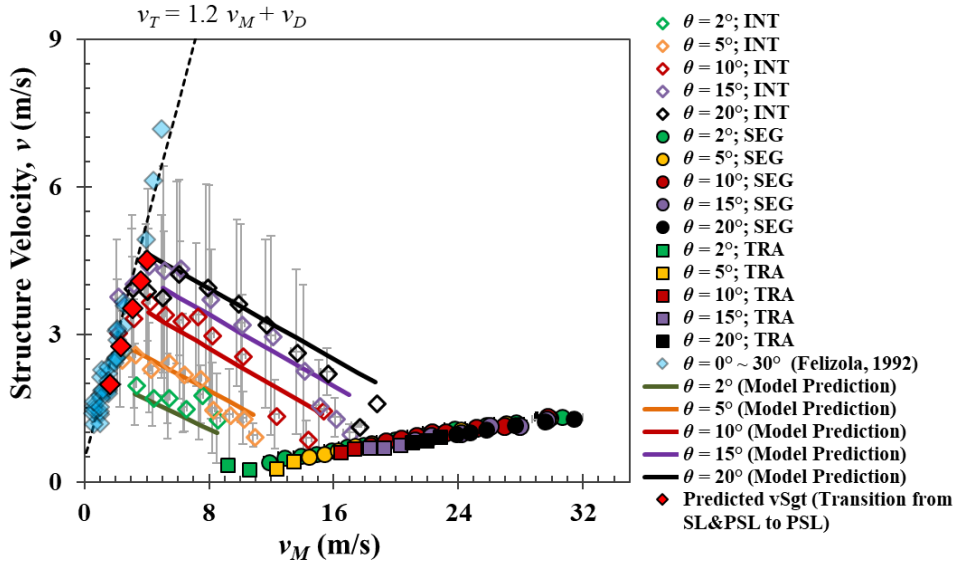

Fig. 22. Comparison between measured and predicted pseudo-slug velocity from the second approach for v_{SL} = 0.005 m/s

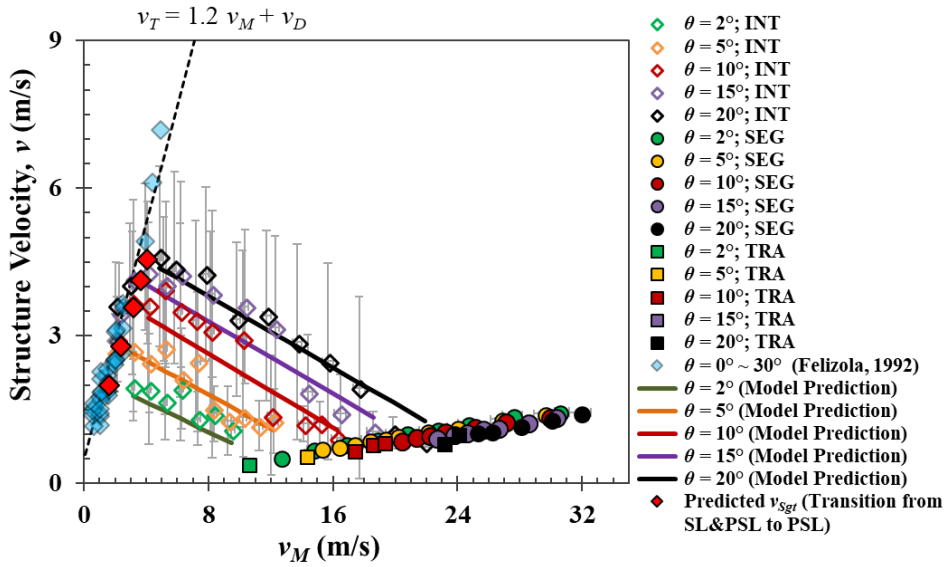

Fig. 23. Comparison between measured and predicted pseudo-slug velocity from the second approach for v_{SL} = 0.01 m/s

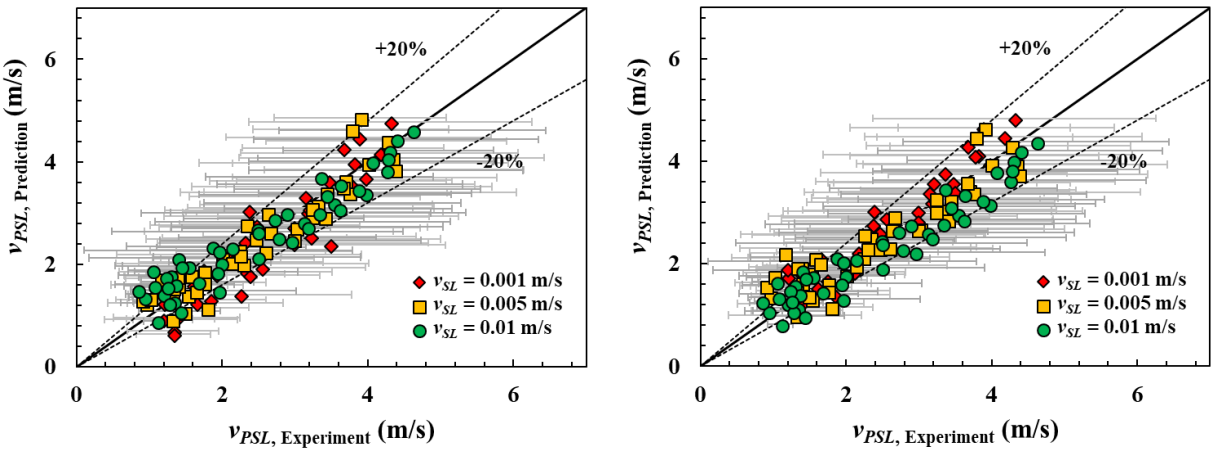

(a). First Approach (b). Second Approach

Fig. 24. Performance of the new model for pseudo-slug velocity prediction in terms of different liquid flow rates

Table 2. Statistical Parameter for the Model Prediction of Pseudo-slug Velocity

Approach\Error	ε_1 (%)	ε_2 (%)	ε_3 (%)	ε_4 (m/s)	ε_5 (m/s)	ε_6 (m/s)
First Approach (v_{SL} = 0.001 m/s)	-8.44	16.11	19.08	-0.15	0.36	0.42
Second Approach (v_{SL} = 0.001 m/s)	-18.87	20.31	16.29	-0.40	0.45	0.34
First Approach (v_{SL} = 0.005 m/s)	3.40	14.14	18.67	0.02	0.28	0.35
Second Approach (v_{SL} = 0.005 m/s)	7.83	18.60	27.08	0.06	0.33	0.41
First Approach (v_{SL} = 0.01 m/s)	8.96	18.17	25.28	0.05	0.31	0.37
Second Approach (v_{SL} = 0.01 m/s)	-2.00	15.79	20.15	-0.16	0.33	0.36
First Approach (Total)	1.31	16.14	21.01	-0.03	0.32	0.38
Second Approach (Total)	-4.35	18.23	21.17	-0.17	0.37	0.37

4. Conclusions

A detailed experimental study was conducted in a 3-in low-pressure facility to investigate the transition region between segregated and conventional slug flow in upward inclined pipes. Tulsa city municipal water and compressed air were used as the test fluids. Three liquid flow rates (0.001, 0.005 and 0.01 m/s) and five inclination angles (2°, 5°, 10°, 15° and 20°) were studied.

Overall, the general flow patterns observed in the uphill section for the current experimental test matrix are segregated flow, intermittent flow and the transition between these two flow patterns. These flow patterns are further divided into several different categories based on the liquid entrainment, liquid wetted perimeter, and flow characteristic. Pseudo-slug flow has been observed between segregated and conventional slug flow. It has been classified into intermittent flow in the current study.

This paper compares pseudo-slug flow with normal slug flow in terms of 1-D liquid holdup evolution, 2-D axial liquid holdup distribution evolution, 2-D cross-sectional liquid holdup distribution, and 3-D interfacial structure. The experimental data show that the cross-sectional area of the pipe cannot be fully blocked by the continuous liquid phase in the pseudo-slug body. There is some gas passing through with a large amount of liquid entrainment. The entrained liquid droplets deposit on the pipe wall and form a liquid film surrounding the pipe wall. Due to the inefficient blockage of the gas passage, the pseudo-slug velocity is less than the one supposed for slug flow.

The current experimental data also show that the flow pattern transition from pseudo-slug to slug flow is gradual, and the structure velocity can be used as an indicator of flow pattern transition. When pseudo-slug flow becomes dominant, the structure velocity deviates from the slug translational velocity due to the insufficient blockage within the pseudo-slug body.

Finally, two simplified correlations for pseudo-slug velocity are proposed. These correlations can be used as closure relationships in any pseudo-slug mechanics model.

Acknowledgement

The authors would like to acknowledge the company members of Tulsa University Fluid Flow Project (TUFFP) for their support in the current research, and Helmholtz-Zentrum Dresden-Rossendorf (HZDR) for their technical support on mire-mesh sensor. The authors also acknowledge Dr. Carlos F. Torres and Mr. Auzan Soedarmo for their fruitful discussion on this

challenging work, and Dr. Tayfun Besim Aydin for his technical support at the beginning of this work.

References

Alsaadi, Y. 2013. *Liquid Loading in Highly Deviated Gas Wells*. MS thesis, University of Tulsa, Tulsa, Oklahoma (December 2013).

Alsaadi, Y., Pereyra, E., Torres, C. and Sarica, C. 2015. Liquid Loading of Highly Deviated Gas Wells from 60° to 88°. Presented at SPE Annual Technical Conference and Exhibition, Houston, Texas, 28-30 September. SPE-174852-MS. https://doi.org/10.2118/174852-MS.

Alves, G.E. 1954. Concurrent Liquid-Gas Flow in a Pipeline Contactor. *Chem. Engng Prog.* 50, 449-456.

Barnea, D. 1987. A Unified Model for Predicting Flow-Pattern Transitions for the Whole Range of Pipe Inclinations. *Int. J. Multiphase Flow* **13** (1): 1-12. https://doi.org/10.1016/0301-9322(87)90002-4.

Barnea, D., Shoham, O. and Taitel, Y. 1980. Flow Pattern Characterization in Two-Phase Flow by Electrical Conductance Probe. *Int. J. Multiphase Flow* **6** (5): 387-397. https://doi.org/10.1016/0301-9322(80)90001-4.

Bendiksen, K. H. 1984. An Experimental Investigation of the Motion of Long Bubbles in Inclined Tubes. *Int. J. Multiphase Flow* **10** (4): 467-483. https://doi.org/10.1016/0301-9322(84)90057-0.

Brito, R. 2015. Effect of Horizontal well trajectory on Two-phase Gas-Liquid Flow Behavior. Ph.D. Dissertation, University of Tulsa, Tulsa, Oklahoma (December 2015).

Brito, R. Pereyra, E., and Sarica, C. 2016b. Effect of Well Trajectory on Liquid Removal in Horizontal Gas Wells. SPE Annual Technical Conference and Exhibition. Dubai, UAE, 26-28 September. SPE-181423-MS. https://doi.org/10.1016/j.petrol.2017.03.042.

Butterworth, D. and Pulling, D. J. 1972. A Visual Study of Mechanisms in Horizontal, Annular, Air-Water Flow. WERE Report M2556, Harwell, Oxon.

Chen, X.T., Brill, J.P., 1997. Slug to churn transition in upward vertical two-phase flow. *Chem. Eng. Sci*. **52** (23): 4269–4272. https://doi.org/10.1016/S0009-2509(97)00178-4.

Ekinci, S. 2015. Pipe Inclination Effects on Slug Flow Characteristics of High Viscosity Oil-Gas Two-Phase Flow. MS thesis, University of Tulsa, Tulsa, Oklahoma.

Fan, Y. 2017. A Study of the Onset of Liquid Accumulation and Pseudo-slug Flow Characterization. Ph.D. Dissertation. U. of Tulsa, Oklahoma (May 2017).

Fan, Y., Pereyra, E., and Sarica, C. 2018. Onset of Liquid Film Reversal in Upward Inclined Pipe. *SPE J*. In Press. SPE-191129-PA. https://doi.org/10.2118/191120-PA.

Fan, Y., Pereyra, E., Torres-Monzon, C. F., Aydin, T. B. and Sarica, C. 2015. Experimental Study on the Onset of Intermittent Flow and Pseudo-slug Characteristics in Upward Inclined Pipes. 17th International Conference on Multiphase Technology, June 10 - 12, 2015, Cannes, France.

Guner, M. 2012. Liquid Loading of Gas Wells with Deviations from 0°to 45°. M.S. thesis, University of Tulsa, Tulsa, Oklahoma.

Guner, M., Pereyra, E., Sarica, C. and Torres, C. 2015. An Experimental Study of Low Liquid Loading in Inclined Pipes from 90° to 45°. SPE Production and Operations Symposium, Oklahoma City, Oklahoma, 1-5 March. https://doi.org/10.2118/173631-MS.

Kipping, R., Brito, R., Scheicher, E. and Hampel, U. 2016. Developments for the application of the Wire-Mesh Sensor in industries. *Int. J. Multiphase Flow* **85**: 86-95. https://doi.org/10.1016/j.ijmultiphaseflow.2016.05.017.

Lee, A.H. 1993. A Study of Flow Regime Transition for Oil-Water-Gas Mixtures in Large-Diameter Horizontal Pipelines. M.S. Thesis, Ohio University, Athens, Ohio.

Lin. P. Y. and Hanratty T. J. 1987a. Detection of Slug Flow from Pressure Measurements. *Int. J. Multiphase Flow* **13** (1): 13-21. https://doi.org/10.1016/0301-9322(87)90003-6.

Lin. P. Y. and Hanratty T. J. 1987b. Effect of Pipe Diameter on Flow Patterns for Air-Water Flow in Horizontal Pipes. *Int. J. Multiphase Flow* **13** (4): 549-563. https://doi.org/10.1016/0301-9322(87)90021-8.

Loh, W.L., Perez, V., Tam, N.D., Wan, T.T., Zhao, Y. and Premanadhan, V.K. 2016. Experimental Study of the Effect of Pressure and Gas Density on the Transition from Stratified to Slug Flow in a Horizontal Pipe. *Int. J. Multiphase Flow* **85**: 196-208. https://doi.org/10.1016/j.ijmultiphaseflow.2016.06.005.

Maley, J. 1997. Slug Flow Characteristics and Corrosion Rates in Inclined High Pressure Multiphase Flow Pipes. MS thesis, Ohio University, Athens, Ohio.

Nicklin, D.J., Wilkes, J.O., Davidson, J.F., 1962. Two-phase flow in vertical tubes. *Trans. Inst. Chem. Eng.* **40**: 61–67.

Nicholson, M. K., Aziz, K. and Gregory, G. A. 1977. Intermittent Two-Phase Flow in Horizontal Pipes: Predictive Models. 27th Canadian Chemical Engineering Conference, Calgary, Alberta.

Prasser, H. -M., Böttger, A., Zschau, J., 1998. A new electrode-mesh tomography for gas–liquid flows. *Flow Meas. Instrum*. **9** (2): 111–119.

Shoham, O. 2006. Mechanistic Modeling of gas-Liquid Two-Phase Flow in Pipes. SPE book.

Soedarmo, A., Soto-Cortes, G., Pereyra, E., Karami, H. and Sarica, C. 2018. Analogous behavior of pseudo-slug and churn flows in high viscosity liquid system and upward inclined pipes. *Int. J. Multiphase Flow* **103**: 61-77. https://doi.org/10.1016/j.ijmultiphaseflow.2018.02.001.

Soleimani, A. and Hanratty, T.J. 2003. Critical Liquid Flows for the Transition from the Pseudo-slug and Stratified Patterns to Slug Flow. *Int. J. Multiphase Flow* **29** (1): 51-67. https://doi.org/10.1016/S0301-9322(02)00124-6.

Taitel, Y. and Dukler, A.E. 1976. A Model for Predicting Flow Regime Transition in Horizontal and Near Horizontal Gas-Liquid Flow. *AIChE J.* **22** (1): 47-55.

Tecplot 360™ User's Manual Version 2013.

Wilkens, R. J. 1997. Prediction of the Flow Regime Transitions in High Pressure, Large Diameter, Inclined Multiphase Pipelines. Ph.D. Dissertation, Ohio University, Athens, Ohio.

Zabaras, G., Dukler, A. E., and Moalem-Maron, D. 1986. Vertical Upward Cocurrent Gas-Liquid Annular Flow. *AIChE J*. **32** (5): 829-843.

Zhang, H.-Q., Wang, Q., Sarica, C., Brill, J.P., 2003b. Unified model for gas-liquid pipe flow via slug dynamics - part 1: model development. *J. Energy Res Technol*. **125** (4), 266–273.

Appendix A: Flow Pattern Map

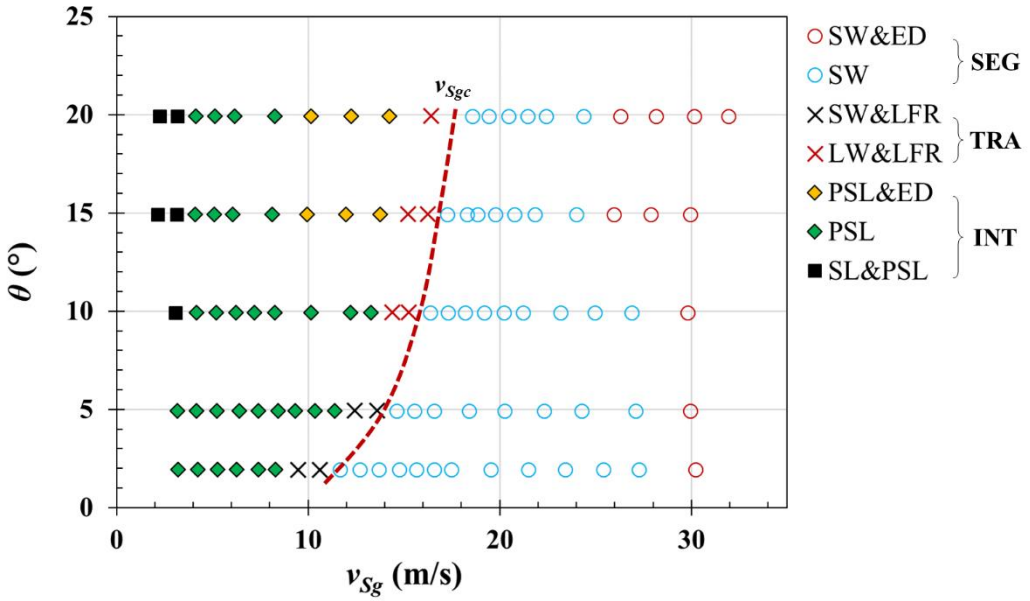

Fig. A-1. Flow Pattern Map for v_{SL} = 0.001 m/s

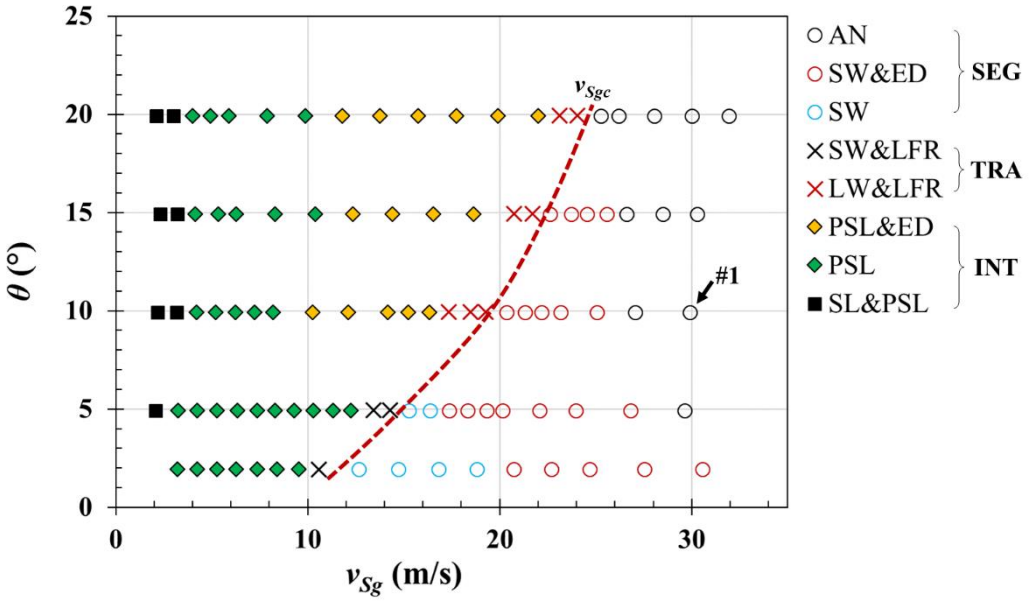

Fig. A-2. Flow Pattern Map for v_{SL} = 0.01 m/s